Quantitative Structure of a Complex between a Minor-Groove-Specific Drug and a Bent DNA Decamer Duplex: Use of 2D NMR Data and NOESY Constrained Energy Minimization†

Mukti H. Sarma,‡ Goutam Gupta,§ Angel E. Garcia,§ Kimiko Umemoto,‡,∥ and Ramaswamy H. Sarma*,‡

Institute of Biomolecular Stereodynamics, Department of Chemistry, State University of New York, 1400 Washington Avenue, Albany, New York 12222, and Theoretical Biology and Biophysico Group, T-10, MS K710, Los Alamos National Laboratory, Los Alamos, New Mexico 87545

Received August 16, 1989; Revised Manuscript Received January 12, 1990

ABSTRACT: Two-dimensional nuclear magnetic resonance (2D NMR) studies on $d(GA_4T_4C)_2$ and $d(GT_4A_4C)_2$ [Sarma, M. H., et al. (1988) *Biochemistry 27*, 3423–3432; Gupta, G., et al. (1988) *Biochemistry 27*, 7909–7919] showed that A·T pairs are propeller twisted. As a result, A/T tracts form a straight rigid structural block with an array of bifurcated inter base pair H bonds in the major groove. It was demonstrated (previous paper) that replacement of methyl group by hydrogen (changing from T to U) in the major groove does not disrupt the array of bifurcated H bonds in the major groove. In this article, we summarize results of 2D NMR and molecular mechanic studies on the effect of a minor-groove-binding A·T-specific drug on the structure $d(GA_4T_4C)_2$. A distamycin analogue (Dst2) was used for this study. It is shown that Dst2 binds to the minor groove of $d(GA_4T_4C)_2$ mainly driven by van der Waals interaction between A·T pairs and the drug; as a consequence, an array of bifurcated H bonds can be formed in the minor groove between amide/amino protons of Dst2 and A·T pairs of DNA. NOESY data suggest that Dst2 predominantly binds at the central 5 A·T pairs. NOESY data also reveal that, upon drug binding, $d(GA_4T_4C)_2$ does not undergo any significant change in conformation from the free state; i.e., propeller-twisted A·T pairs are still present in DNA and hence the array of bifurcated H bonds must be preserved in the major groove. NOESY data for the A5-T6 sequence also indicate that there is little change in junction stereochemistry upon drug binding.

It is well-known that the presence of A/T tracts at regular intervals of 10 base pairs in a DNA polymer can cause macroscopic DNA bending (Hagerman, 1985; Koo et al., 1986; Marini et al., 1982). It is also known that the dimer sequence connecting two neighboring A/T tracts is extremely important; the cases in point are two Hagerman polymers, i.e., poly[$d(GA_4T_4C)_2$] is bent while poly[$d(GT_4A_4C)_2$] is straight (Hagerman, 1986). These studies suggested that two factors primarily contribute to the observed bending in DNA polymers with A/T tracts: (i) the structural pecularity of the A/T tract and (ii) the stereochemistry of the dimer sequence that connects two neighboring A/T tracts. However, details about these two structural aspects could not be obtained from the experimental studies on macroscopic DNA bending because the techniques used in these studies (gel electrophoresis, electron microscopy, etc.) could only provide information at the macroscopic level. In an attempt to visualize the structural roles of the A/T tracts and the junction sequence on DNA bending, we initiated two-dimensional nuclear magnetic resonance (2D NMR) studies on two decamers, $d(GA_4T_4C)_2$ and $d(GT_4A_4C)_2$. The results of these studies were previously reported (Sarma et al., 1988; Gupta et al., 1988). These studies revealed that in both decamers the A·T base pairs are propeller twisted and this can lead to an array of inter base pair bifurcated H bonds in the major groove involving N6 of A and O4 of T belonging to two neighboring A·T pairs inside the A/T tract. It was also demonstrated that there is a small but finite (detectable by NMR) structural difference between $d(GA_4T_4C)_2$ and $d(GT_4A_4C)_2$; a junction is created when two A/T tracts are jointed at the A-T sequence in $d(GA_4T_4C)_2$ while when two A/T tracts are connected by a T-A sequence [in $d(GT_4A_4C)_2$] no discontinuity is observed. Thus, our structural studies based on the NMR data provide a simple explanation of why two Hagerman polymers, poly[$d(GA_4T_4C)_2$] and poly[$d(GT_4A_4C)_2$], are electrophoretically different: they are different because the two decamer repeats are structurally different. Subsequent to our NMR studies, Chen et al. (1988) performed high-resolution electrophoresis on $d(GA_4T_4C)_2$ and $d(GT_4A_4C)_2$; they showed that $d(GA_4T_4C)_2$ is electrophoretically retarded while $d(GT_4A_4C)_2$ is normal.

Use of a full-matrix NOESY simulation technique with respect to the observed data at various mixing times enabled us to describe the structures of $d(GA_4T_4C)_2$ and $d(GT_4A_4C)_2$ in terms of the conformations of each constituent nucleotide (Sarma et al., 1988; Gupta et al., 1988). Thus, we are in a position to monitor the structural changes (at the nucleotide level) in the parent structures as caused by DNA-binding ligands. Of particular importance was the decamer $d(GA_4T_4C)_2$, which exhibits a bent junction B-DNA model in solution (Sarma et al., 1988). It was of interest to examine whether a minor-groove-specific ligand/drug smooths the structural discontinuity at the A-T junction. For this purpose we chose a distamycin analogue with two pyrrole rings (henceforth called Dst2)–a groove-binding drug specific for

† This work is supported by the U.S. Department of Energy, by grants from the National Institutes of Health (GM29787), and by a contract from the National Foundation of Cancer Research. The high-field NMR experiments were performed at the NMR facility for Biomolecular Research located at the Francis Bitter National Magnet Laboratory, MIT. The NMR facility is supported by Grant PR0095 from the Division of Research Resources of the NIH and by the National Science Foundation under Contract C-670.

‡ State University of New York.

§ Los Alamos National Laboratory.

∥ Permanent address: Department of Chemistry, International Christian University, Mitaka, Tokyo 181, Japan.

0006-2960/90/0429-4723$02.50/0

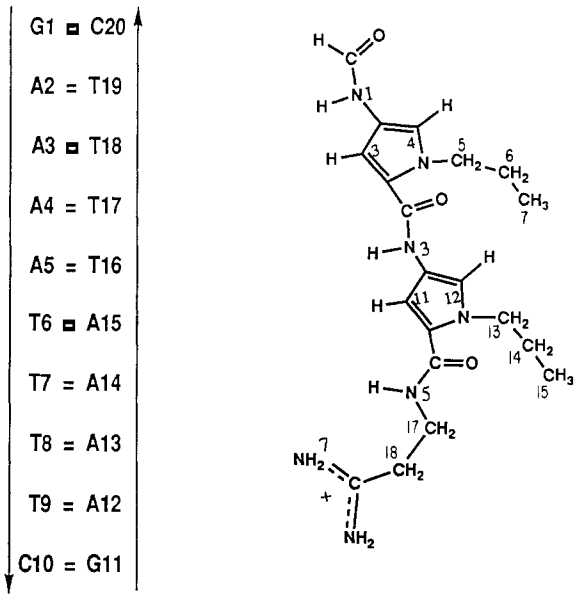

FIGURE 1: Numbering of the residues in the duplex $d(GA_4T_4C)_2$. Numbering of the atoms in the distamycin analogue (Dst2) is also indicated. Note that the amide (N1, N3, N5), amino (N7), and pyrrole ring HC3/HC11 protons fall on the concave surface of the molecule.

A·T pairs (see Figure 1 for the chemical structure of the drug). In this article, we present the results of our NMR studies on the Dst2–$d(GA_4T_4C)_2$ complex (1:1) and we also discuss the possible implications of our results in DNA bending. We combined experimental 1D/2D NMR techniques with various theoretical methods including NOESY simulations and molecular mechanics calculations to arrive at a detailed description of the structural features of the drug–DNA complex.

Materials and Methods

The drug Dst2 was a gift from Drs. A. Ahuze, A. Zasedatelev, and G. Gursky of the Institute of Molecular Biology, Academy of Sciences of USSR. Details of the synthesis and purification scheme of the decamer $d(GA_4T_4C)_2$ were given in our previous paper (Sarma et al., 1988).

NMR Spectroscopy. For both H_2O and D_2O samples Dst2 and $d(GA_4T_4C)_2$ were mixed in 1:1 molar ratio; the DNA concentration was 2 mM in duplex in 20 mM phosphate buffer with 2 mM EDTA and 100 mM NaCl (pH = 7.5). 1D NMR spectra of the drug–DNA complex in H_2O were recorded by using a time-shared long-pulse sequence in the temperature range of 10–25 °C. NOE difference spectra were recorded at 12 °C for presaturation (τ_m) of 100 and 200 ms with a relaxation delay (RD) of 1.2 s and number of transients (NS) of 5000. The COSY spectrum of the drug Dst2 was collected at 22 °C in the pure absorption mode (States et al., 1982) with the pulse sequence $(RD\text{-}90°\text{-}t_1\text{-}90°\text{-}Acq)_{NS}$ with RD = 1.2 s and the data matrix (t_1 = 1024 × t_2 = 512) for NS = 48. NOESY spectra of the Dst2–$d(GA_4T_4C)_2$ complex in D_2O were recorded at 22 °C by using the pulse sequence $(RD\text{-}90°\text{-}t_1\text{-}90°\text{-}\tau_m\text{-}90°\text{-}Acq)_{NS}$ with RD = 1.2 *NS* = *64* and τ_m = 50, 100, and 150 ms. NOESY data were also collected in the pure absorption mode (States et al., 1982).

Structure Determination from NOESY Data. We arrived at the structure of the drug–DNA complex in the following manner. *Step 1.* Full-matrix NOESY simulations were performed following the principle of Keepers and James (1984); for details of applications, see Gupta et al. (1988); and Broido et al. (1985). Drug protons were not included in the simulations and theoretical NOESY intensities were computed and compared with the corresponding observed values at τ_m = 50, 100, and 150 ms for all pairwise interproton interactions. An isotropic correlation time of τ_c = 3 ns was used. By use of a low *R*-factor criterion, i.e., *R* factor values less than or equal to 0.15, a stereochemically satisfactory model was obtained for the DNA in the Dst2–$d(GA_4T_4C)_2$ (1:1) complex.

Table I: Assignment of the Nonexchangeable DNA Protons in Dst2–$d(GA_4T_4C)_2$ (1:1) in D_2O at 22 °C[a]

residue	H8/H6	H2/H5/CH$_3$	H1′	H2′	H2″	H3′
G1	7.84		5.48	2.41	2.62	4.80
A2	8.19	7.43	5.78	2.70	2.82	5.03
A3	8.11	7.24	5.78	2.70	2.82	5.03
A4	8.02	7.36	5.78	2.62	2.82	4.99
A5	8.06	7.89	5.91	2.45	2.80	4.99
T6	7.04	1.25	5.80	1.87	2.39	4.61
T7	7.35	1.51	5.80	2.06	2.47	4.60
T8	7.40	1.68	6.24	2.07	2.25	4.60
T9	7.44	1.63	6.24	2.04	2.28	4.60
C10	7.59	5.72	5.48	2.27	2.45	4.57

[a] Chemical shift (ppm) values are given with respect to TSP as an internal standard.

1D slices through the following signals are chosen for experimental NOESY intensity measurements: H8/H6 (G1, A2, A3, C10, T6), H2/H5/CH3 (A3, A5, T6, T7, C10), H1′ (G1, C10, A5), and H3′ (G1) (Table I). In most of these cases, the NOE source peaks and/or the NOE cross peaks were not overlapping or only mildly overlapping. Note that even though the H1′s of G1 and C10 overlap they are treated separately since the NOESY pathways from these two signals do not interfere because they are >10 Å away. The pair H2′,H2″ is treated as nonoverlapping when both H2′ and H2″ did not show overlap with other signals. Nonoverlapping H2′,H2″ pairs are due to G1, A4, T6, T7, and C10 (Table I). For all these protons NOESY slices could be taken through them or NOESY intensities can be measured to obtain the experimental peak heights a^o_{ij} (due soley to one pairwise interaction) used in the structure refinement (and *R*-factor calculation) by using the full-matrix NOESY simulation. NOESY slices through each of 19 nonoverlapping slices at a given τ_m show 3–6 NOE sites (Figure 8); therefore, from each NOESY experiment we have ~70 independent NOESY intensities. In the present case NOESY experiments were performed at three τ_m (i.e., 50, 100, and 150 ms). Thus, we have in all about 70 × 3 = 210 observed intensities for pairwise interactions and these were only used for *R*-factor calculations. In addition, the 1D NOE data in H_2O (τ_m = 100 and 200 ms) (Figures 2 and 3) are used to obtain the gross morphology of $d(GA_4T_4C)_2$ in the complex (Gupta et al., 1988).

Step 2. NOESY simulations resulted in a structural model for the DNA in the drug–DNA complex. From this model ~60 interproton distances involving DNA protons were extracted out and taken out as structural constraints required for agreement with the NOESY data. With these constraints the drug–DNA complex was energy minimized in the Cartesian coordinate space by using the force fields of Wiener et al. (1982); all atoms (including hydrogens) in the drug and in the DNA were included. Dst2 force-field parameters are derived from the netropsin parameter file in the AMBER package. The charges in the neutral end group of Dst2 were appropriately modified and the parameters for the $-CH_2-CH_2-CH_3$ were taken also from the AMBER parameter library. The Dst2–$d(GA_4T_4C)_2$ contacts were not included as constraints during energy minimization. The fact that the drug–$d(GA_4T_4C)_2$ contacts are in agreement with the observed NOESY pattern involving Dst2 and DNA protons shows that experimental mode of drug binding is also energetically fea-

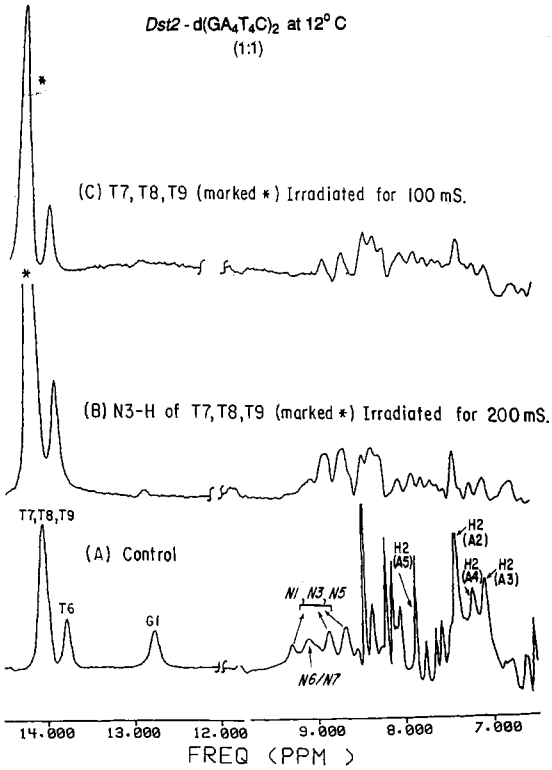

FIGURE 2: 1D NMR spectra of the Dst2–d(GA_4T_4C)$_2$ (1:1) complex in H_2O at 12 °C. DNA concentration, 2 mM in strand; salt, 100 mM in NaCl in 20 mM sodium phosphate buffer with 2 mM EDTA (pH 7.5). Spectra were recorded by using a time-shared long-pulse sequence. (A) Control spectrum: signals from imino protons of Watson–Crick A·T pairs are located at 14.08 (for A2-T19/A12-T9, A3-T18/A13-T8, and A4-T17/A14-T7) and 13.80 ppm (for A5-T16/A15-T6). The imino proton of the Watson–Crick G1-C20/G11-C10 is also located at 12.78 ppm. In addition, H-bonded amide (N1, N3, N5) and amino (N7) protons appear within 9.30–8.50 ppm in the Dst2–d(GA_4T_4C)$_2$ (1:1) complex in H_2O at 12 °C. Nonexchangeable H2 protons of A2/A12, A3/A13, A4/A14, and A5·A15 are also indicated. (B) and (C) 1D NOE spectra in which the imino proton signals at 14.08 ppm (for A2-T19/A12-T9, A3-T18/A13-T8, A4-T17·A14-T7) are irradiated for τ_m = 200 and 100 ms. Note that H2 of A2, A3, and A4 appear as sites of NOE.

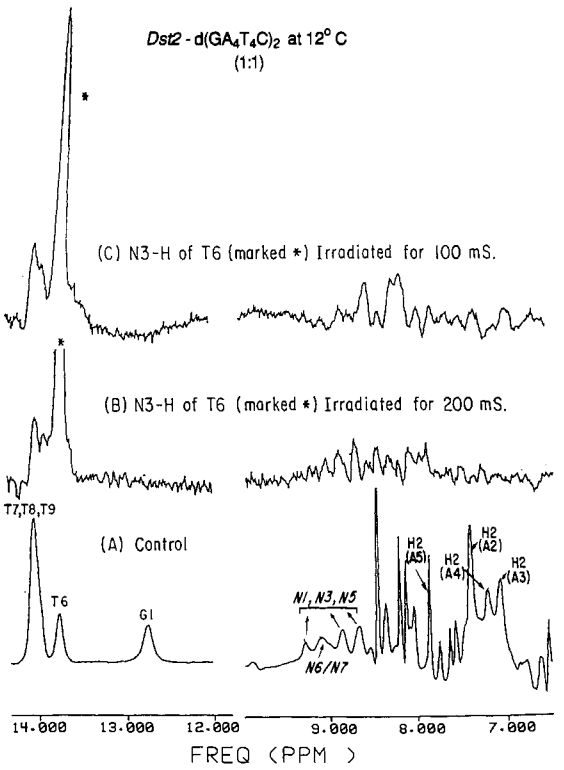

FIGURE 3: 1D NMR spectra of the Dst2–d(GA_4T_4C)$_2$ (1:1) complex in H_2O at 12 °C (solution conditions are the same as in Figure 2). (A) Control spectra in which the imino proton signal at 13.80 ppm is irradiated for τ_m = 200 and 100 ms.

sible. The B-DNA model of Arnott and Hukins (1972), and not the NMR model, was chosen as the starting structure for constrained energy minimization. This was done for the following reason. NOESY data provide information about a set of interproton distances from which we can deduce sugar pucker given by torsion angle δ, glycosyl torsion χ, and base parameters (Gupta et al., 1988). But from the NOESY data we have no direct information about other backbone torsion angles, i.e., α, β, γ, ϵ, and ζ [for nomenclature, see Saenger (1984)]. In NOESY simulation (Gupta et al., 1988) we constrained δ, χ, and base parameters within a range of values to satisfy the NOESY data and varied other torsion angles (i.e., α, β, γ, ϵ, and ζ) to obtain stereochemically acceptable models. A DNA model so obtained after NOESY simulation is only one of the possible structures in the multidimensional conformation space that satisfy NOESY data. Therefore, constrained energy minimization using the NMR model as the starting structure would artificially bias the final energy-minimized structure in the neighborhood of the starting structure in which the distance criterion is well satisfied to begin with. It was our interest to examine the similarity of the NOESY-simulated model to that we obtain by performing (NOESY) constrained energy minimization of reported B DNA. Arnott and Hukin's B-DNA model was the starting structure of choice because in this structure interproton distances are far removed from those required by NOESY data. Minimization of this model was likely to involve a somewhat unbiased search of the conformational space and this made the comparison of the end results of (NOESY) constrained minimization and NOESY simulation a meaningful exercise.

In compliance with the NMR data, Dst2 was docked in the minor groove and approximately at the center of d(G1-A2-A3-A4-A5-T6-T7-T8-T9-C10)$_2$. In the initial stage of minimization Dst2 amide protons (N1, N3, and N5 in Figure 1) were constrained to form bifurcated H bonds with N3(A) and O2(T) of the base pairs at the center of the DNA duplex; but during the later stages of minimization these drug–DNA constraints were released. At the end of constrained energy minimization, an energetically stable model of the drug–DNA complex was obtained and the model was consistent with the observed NOESY data. Agreement of the energy-minimized Dst2–d(GA_4T_4C)$_2$ complex with respect to the observed NOESY data at τ_m = 50, 100, and 150 ms was reconfirmed by performing NOESY simulation (and the associated *R*-factor test); at this stage both drug and DNA protons were included in the simulation. The same correlation time of τ_c = 3 ns was used for drug and DNA protons.

Line-Shape Analysis. When two or more protons overlap at one NOE site it is difficult to experimentally obtain the individual NOEs corresponding to each overlapping proton. Hence, under such a situation we resorted to a line-shape analysis in which the contribution of a proton (either the source or site of NOE) to the NOESY slice at a chemical shift value is computed as

$$F_{ij} = 2a^c_{ij}\frac{\exp(-\Delta x^2/0.9\Gamma^2)}{1 + \exp(-\Delta x^2/0.9\Gamma^2)} \quad (1)$$

where a^c_{ij} is the calculated intensity of the NOE at j due to

i by full-matrix NOESY simulation; $\Delta x = x_0 - x$; x_0 is the chemical shift value of the jth proton; x is the chemical shift value at which the contribution of the jth proton to the whole NOESY slice is computed; and Γ is the half line width. Γ is not a variable parameter for NOESY simulation (and related R-factor calculation). The estimate of Γ for the overlapping peaks is obtained from the nonoverlapping peak of the same type, i.e., Γ for the overlapping H8/H6 is obtained from the corresponding value of the nonoverlapping H8/H6 and similarly for H5/H2/CH_3, H1′, etc. The factor 2 (in the numerator) and 0.9 (in the exponent) are the normalizing factors.

Expression 1 allows us to compute the theoretical NOESY slice with contributions from all possible NOE sites and compare it with the corresponding experimentally observed one.

In summary, it may be pointed out that the structural model for the drug–DNA complex was obtained by two methods. *In one method*, "full-matrix NOESY simulation" was performed to obtain a stereochemically acceptable model consistent with the NOESY data. *In another method*, NOESY distance constrained energy minimization was carried out to select an energetically stable model consistent with the NOESY data.

Results

Exchangeable Protons of the Drug and the DNA. Figures 2 and 3 show 1D NMR spectra of the Dst2–d(GA_4T_4C)$_2$ complex (1:1) at 12 °C in H_2O. Watson–Crick imino (NH) protons are located within 14.20–12.70 ppm as three signals at 14.08, 13.80, and 12.78 ppm. Sequential assignment of the NH protons was achieved by performing 1D NOE by irradiating three NH signals at presaturation times of 100 and 200 ms and by comparing the corresponding NOE pattern in free DNA (Sarma et al., 1988). The signal at 12.78 ppm is assigned to N1–H of G1·C20/G11·C10 (see Figure 1 for the numbering scheme of bases in the duplex). The signal at 13.80 ppm is identified as N3–H of A5·T16/A15·T6 and the remaining N3–H of the A·T pairs are located at 14.08 ppm. Absence of resonance doubling of the NH signals implied that both strands were conformationally equivalent even in the presence of the drug. The NOE pattern in the base proton region of 8.50–7.00 ppm (Figures 2 and 3) enabled us to sequentially assign H2 of A's. See Table I for the chemical shift values. Four distinct signals are seen within 9.30–8.50 ppm; these signals are not present either in the D_2O sample or in the H_2O sample of the free DNA under the same condition (Sarma et al., 1988). This implies that these signals are the exchangeable protons from Dst2, i.e., amide protons of N1, N3, and N5 and amino protons of N6 and N7 (see Figure 1 for the numbering scheme). For DNA oligomer complexes of regular netropsin (Gupta et al., 1984, 1985), exchangeable drug protons were located within a similar ppm range. Observation of exchangeable Dst2 protons suggests that they are involved in H bonding within the Watson–Crick A·T pairs in the minor groove of DNA. We made no attempt to separately identify these four signals at 9.28, 9.06, 8.90, and 8.67 ppm; however, it is rather obvious that the broad signal at 9.06 ppm should originate from the amino proton(s) of N6/N7 (Figure 1). Note that irradiation of the N3–H of the A·T pairs shows small nonspecific NOEs at the exchangeable drug protons. This is not a primary NOE because the stereochemistry of Dst2 binding in the minor groove requires that N3–H of the A·T pairs be ≥3.7 Å away from the amide (N1, N3, N5) and amino (N7) protons of Dst2 (see later in the text). Observed nonspecific NOEs between N3–H of the A·T pairs and drug protons (N1, N3, N5, N7) probably originate due to chemical exchange and/or second-order NOE via H2 of A's which are 2.5–3.5 Å away from the N3–H of the A·T pairs in the Dst2–d(GA_4T_4C)$_2$ complex.

Note that 1D NMR experiments in H_2O were done to establish the fact that the amide (and possibly amino N7) protons of Dst2 are involved in H bonding with the A·T pairs in DNA. All the quantitative structural details were obtained from NOESY data of the complex in D_2O at 22 °C. A lower temperature 12 °C (and not 22 °C) was chosen for H_2O experiments (1D NOE) because at higher temperature (22 °C) we encountered a lot of chemical exchange. But by monitoring the exchangeable protons within 12–25 °C we made sure that the same intact complex existed throughout the temperature range.

Assignment of Nonexchangeable DNA Protons in the Complex. Previously we reported the complete assignment of nonexchangeable DNA protons of d(GA_4T_4C)$_2$ in D_2O at 12 °C (Sarma et al., 1988). We monitored the change in chemical shift in these protons upon raising the temperature to 22 °C and upon subsequent drug binding at 22 °C. From 1D NOE experiments of the Dst2–d(GA_4T_4C)$_2$ complex in D_2O at 12 °C we could locate the positions of H2 of A and by monitoring the temperature-induced change we concluded that at 22 °C H2 protons are located as follows: H2(A2) at 7.43, N2(A3) at 7.24, H2(A4) at 7.36, and H2(A5) at 7.89 ppm. Examinations of NOESY data of the complex for τ_m = 50, 100, and 150 ms suggested that DNA adopts the gross morphology of a right-handed B DNA as in the free DNA (Sarma et al., 1988). A typical cross-connectivity pattern for B DNA is H2″ $(i-1) \xrightarrow{2.4\text{ Å}}$ H8/H6(i) $\xrightarrow{2.4\text{ Å}}$ H2″ (i) →, and so on. Hence, once a marker residue is located, it is possible to sequentially assign H8/H6, H2′,H2″ from the H8/H6 vs H2′, H2″ cross section. Figure 4A shows the H8/H6 vs H2′,H2″ cross section of Dst2–d(GA_4T_4C)$_2$ for τ_m = 150 ms. In this connectivity route H2″(A5)–H6(T6) is easily isolated because this is the only cross peak expected between purine and pyrimidine residues. With T6 as a marker, the sequential assignment of H8/H6, H2′,H2″ is readily obtained. This cross section (Figure 4A) also allows the sequential assignment of CH_3 of T because of the presence of H6(T_i) $\xrightarrow{3.4\text{ Å}}$ $CH_3(T_{i+1})$ $\xrightarrow{3.0\text{ Å}}$ H6(T_{i+1}) →, and so on. Figure 4B shows the H2′,H2″ vs H1′ NOESY cross section for the complex for τ_m = 150 ms. By combination of 4A and 4B, the sequential assignment of H8/H6, H1′, H2′, and H2″ is obtained. In Dst2–d(GA_4T_4C) (1:1) complex H1′–H8/H6 cross peaks are relatively weak and not observed for all the residues in the DNA molecules, as is evident from the H8/H6 vs H1′ NOESY cross section in Figure 4C. Hence, based upon the results of Figure 4A and B, the expected cross-connectivity route is shown; note that the H1′–H8 peaks are more prominently observable than those corresponding to H1′–H6 peaks. The sequential assignment of H3′ is obtained from the H2′,H2″ vs H3′ cross section [data not shown]. Parts A–C of Figure 5 show H8/H6 vs H2′,H2″, H1′ vs H2′,H2″, and H8/H6 vs H1′ cross sections for Dst2–d(GA_4T_4C)$_2$ (1:1) at τ_m = 100 ms. Following the assignment scheme as mentioned above, we arrive at the same sequential assignment of H8/H6, H2, H5/CH_3, H1′, H2′, H2″, and H3′ spin system. The sequential assignments of H8/H6, H2, H5/CH_3, H1′, H2′, H2″, and H3′ are listed in Table I.

Assignment of the Nonexchangeable Drug Protons in the Complex. Assignment of the nonexchangeable protons in free Dst2 was obtained from the COSY experiment of the free drug in D_2O at 22 °C. By use of the numbering in Figure 1, the chemical shift values (ppm) are as follows: CH_3 (7/15) =

0.80, CH_2 (6/14), = 1.70, CH_2 (5/13) = 4.21, CH_2 (18) = 2.76, CH_2 (17) = 3.72, HC3/C11 = 6.80, HC4/C12 = 7.25. Upon binding to DNA only three sets of protons underwent change in chemical shift values, i.e., in the complex HC3/C11 = 6.67, HC4/HC12 = 7.75/7.61, and CH_3 (7/15) = 1.00; all the other protons remained at the same chemical shift values as in the free drug. Note that upon binding to DNA the degeneracy of the pyrrole ring protons on the convex surface, i.e., HC4/HC12, is lifted.

Dst2 Binds at the Center of the Minor Groove of d-(GA_4T_4C)$_2$. The drug Dst2 can span 5 A·T base pairs (bps) in the minor groove. Hence, Dst2 can choose any successive 5 bps in the stretch of 8 A·T bps in DNA (see Figure 1). In this section, we provide experimental evidence that Dst2 binds predominantly to the central 5 bps in the duplex, i.e., either to

A4 – A5 – T6 – T7 – T8
T17–T16–A15–A14–A13

or to its 2-fold equivalent

A14–A15–T16–T17–T18
T7 – T6 – A5 – A4 – A3

Figure 6 shows the sequence-specific change in chemical shift of the H8/H6, H2, and H1′ protons of DNA upon Dst2 binding. H2 of A4,A5 are down-field shifted, H6 (T6) is high-field shifted and H1′ of A5, T6, and T7 are high-field shifted. Other protons in the H8/H6/H2,H1′ region show very little change in chemical shift. This is a qualitative indication that Dst2 is located at the central 5 A·T bps as shown in Figure 6 and Dst2 forms bifurcated H bonds in the minor groove.

Figure 7 provides quantitative evidence that Dst2 spans the central 5 A·T pairs in the Dst2–d(GA_4T_4C)$_2$ (1:1) complex. NOESY cross peaks involving HC3/HC11 of Dst2 and H2,H1′ of DNA are shown for mixing times τ_m = 50, 100, and 150 ms. Note that, at the lowest τ_m = 50 ms, the most prominent drug–DNA interaction involves HC3/HC11 and H2 of A5 and weak NOESY cross peaks are seen for HC3/HC11 and H1′ (T6,T7) interactions. At τ_m = 50 ms for Dst2–d(GA_4T_4C)$_2$ (1:1) we essentially observe the primary NOESY pattern, and by comparison of the intensities of H6–H5 (C10) (fixed at 2.5 Å) and HC3/HC11–H2(A5), it appears that the HC3/HC11–H2(A5) cross peak appears due to primary NOE and should be less than 3 Å in distance. With increasing τ_m = 100 ms, HC3/HC11–H1′(T6,T7) grows in intensity and compares in intensity with intranucleotide H1′–H6 cross sections. Hence, we conclude that HC3/HC11–H1′(T6,T7) should be ~3.6 Å (average intranucleotide H1′–H6 distance, 3.7 Å). This is only consistent with the mode of binding in which Dst2 spans the central 5 A·T bps in the minor groove as shown in the diagram. In this mode of binding the HC3/HC11–H2(A5/A15) distance can range from 2.2 to 2.7 Å and the HC3/HC11–H1′(T6/T16,T7/T17) can range from 3.2 to 3.7 Å. Upon increasing τ_m to 150 ms, we notice an additional cross peak (absent in the τ_m = 50 and 100 ms cross section) for HC3/HC11–H2(A3/A13,A4/A14)—this peak can either originate from spin-diffusion HC3/HC11 $\xrightarrow{2.5\text{ Å}}$ H2(A5/A15) $\xrightarrow{3.4\text{ Å}}$ H2(A4/A14) → H2(A3/A13) or be due to a minor population of the complex bound to

A2 – A3 – A4 – A5 – T6
T19–T18–T17–T16–A15

This minor population may be in rapid dynamic equilibrium with the major population of the complex as shown in Figures 6 and 7. While interpreting the NOE data, we did not include the effect of minor populations because we believe that such populations are too small to alter our conclusions regarding the prominent binding mode.

Hence, from the results of Figures 6 and 7, we prove that Dst2 predominantly binds at the central 5 bps. As shown in Figure 1, the two end groups of Dst2 are chemically different. Therefore, Dst2 can flip and bind to the same 5 A·T bps without altering the results of Figures 6 and 7 and the H-bonding network in the minor groove. From NMR data we cannot distinguish these two possibilities.

Determination of Three-Dimensional Structure of Dst2–d(GA_4T_4C)$_2$ (1:1) Complex. NMR data presented in Figures 2–7 can be summarized as follows:

(i) Amide protons (N1, N3, N5) and amino (N7) protons of Dst2 are involved in H bonding with d(GA_4T_4C)$_2$ in the (1:1) drug–DNA complex (Figures 2 and 3).

(ii) Upon binding to Dst2, the DNA duplex does not undergo any significant structural change from the free state, i.e., the DNA duplex adopts the gross morphology of a right-handed B DNA with all nucleotides in C2′-endo,anti domain (Sarma et al., 1988).

(iii) In the complex, A·T pairs are propeller twisted as in free DNA, and hence, an array of bifurcated H bonds is retained in the major groove, even in presence of Dst2.

(iv) NMR data (Figures 6 and 7) indicate that Dst2 predominantly binds at the central 5 A·T bps in the decamer.

(v) Examination of NOESY slices through the base H8/H6 protons indicates that at τ_m = 50 ms (showing primary NOE) inside the A/T tract the intranucleotide NOE H8/H6(i)–H2′(i) is stronger than the internucleotide NOE H8/H6-(i)–H2″ (i – 1) but at A5-T6 H6(T6)–H2′(T6) and H6-(T6)–H2″(A5) NOEs are of equal magnitude. The same NOE feature was observed in free d(GA_4T_4C)$_2$ (Sarma et al., 1988).

This structural information was utilized to obtain a three-dimensional structure of the Dst2-d(GA_4T_4C)$_2$ (1:1) complex by the following steps.

Step 1. NOESY (τ_m = 50, 100, 150 ms) cross-peak intensities involving DNA protons were extracted out. We then carried out a full-matrix NOESY simulation and associated *R*-factor test to obtain a structural model of DNA in the Dst2–d(GA_4T_4C)$_2$ (1:1) complex. In this simulation, an isotropic correlation time (τ_c) of 3 ns was used and Dst2 protons were excluded from the relaxation matrix (inclusion of Dst2 protons does not significantly alter the DNA NOESY pattern). The NOESY pattern of DNA protons in the complex and in the free state being very similar, NOESY simulation resulted in a DNA model of d(GA_4T_4C)$_2$ in the complex that is structurally very close to free DNA (Sarma et al., 1988). The structural features are as follows:

(i) A·T pairs are propeller twisted, giving rise to an array of bifurcated H bonds in the major groove of A·T tract.

(ii) The A/T tract is straight and rigid; inside the A/T tract successive A·T pairs are helically rotated by 35° and translated by 3.3 Å.

(iii) All residues (A, G, C, T) in d(GA_4T_4C)$_2$ in the complex belong to the C2′-endo,anti domain.

(iv) At the A5-T6 sequence, there is a structural discontinuity, i.e., local frames of reference of two neighboring A/T tracts do not coincide at A5-T6; a similar feature was observed in free d(GA_4T_4C)$_2$ (Sarma et al., 1988); relative shift parameters are $|\Delta X|$ = 0.3, $|\Delta Y|$ = 0.1, $|\Delta Z|$ = 0.5.

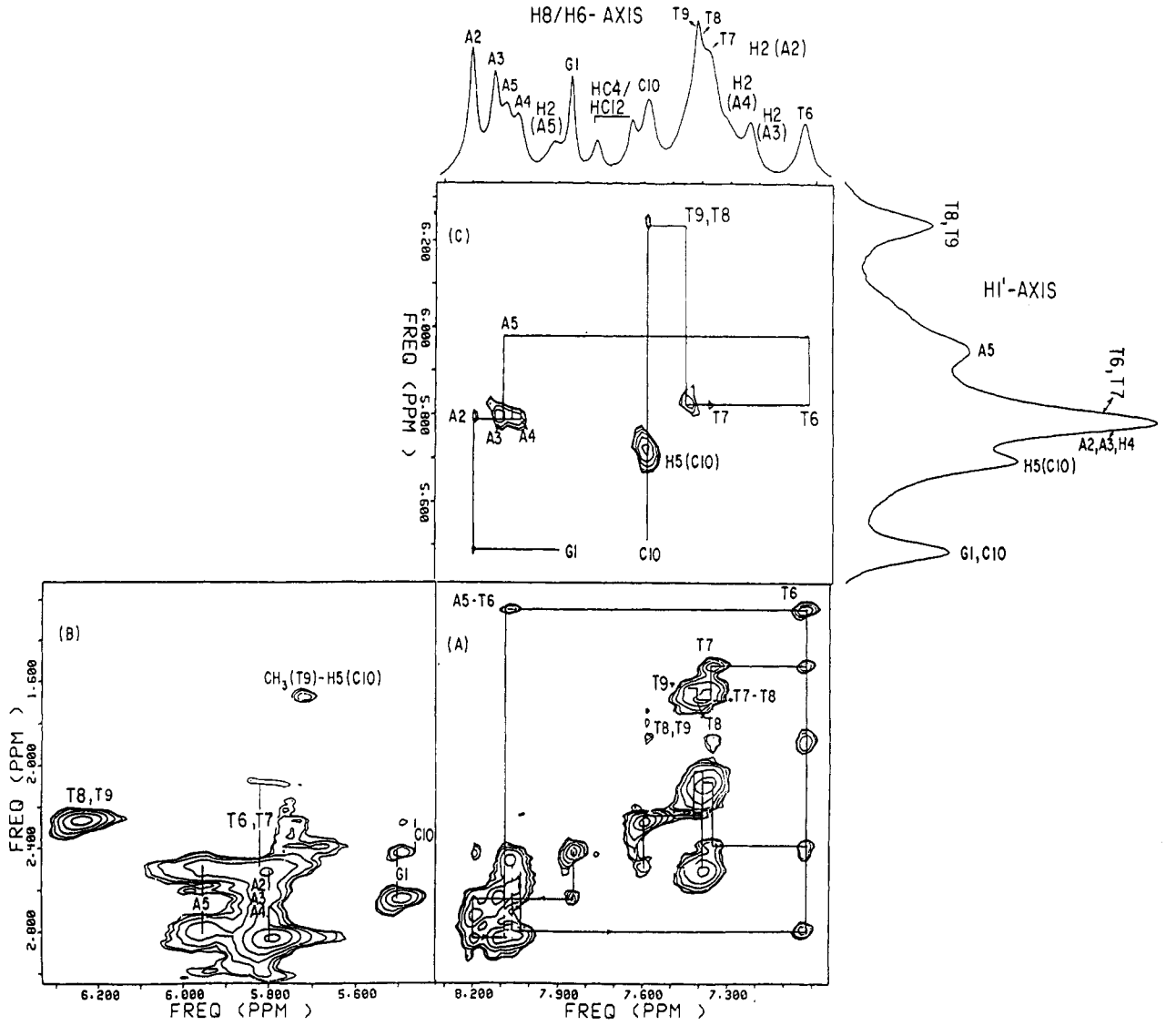

FIGURE 4: NOESY spectra for τ_m = 150 ms of the Dst2–d(GA_4T_4C)$_2$ (1:1) complex in D_2O at 22 °C; other solution conditions are the same as in Figures 2 and 3. By monitoring the NOESY cross peaks from H8/H6 to H1′,H2′,H2″,H3′ as a function of mixing time it was concluded that the DNA in the duplex adopted a gross morphology of a right-handed B-DNA double helix. Three NOESY cross sections were used to establish the sequential assignment of H8/H6, H1′,H2′,H2″ cross section which shows H2″(i − 1) → H8/H6(i) → H2′(i) → H2″(i) → cross-connectivity route in a right-handed B DNA (Sarma et al., 1988; Gupta et al., 1988). This helps sequential assignment of the H8/H6, H2′H2″ spin system and also the CH_3 groups of T. (B) H1′/H5(C) vs H2′,H2″ cross section. Combination of (A) and (B) allows us to sequentially assign the H8/H6, H5,H1′,H2′,H2″ spin system. Sequential assignments of H3′ protons are made from the H2′,H2″ vs H3′ NOESY cross section (data not shown). (C) H1′,H5(C) vs H8/H6 cross section.

The NMR model after NOESY simulation of d(GA_4T_4C)$_2$ in the complex is one of the stereochemically allowed structures in the conformational space. Intranucleotide NOE involving H8/H6, H1′, H2′, H2″, and H3′ provide direct information about sugar pucker (defined by δ) and glycosyl torsion χ. Internucleotide NOEs contain information about the spatial relation of nucleotides (conformations of which are known from intranucleotide NOE) that requires adjustment of α, β, γ, ϵ, and ζ (in addition to δ and χ). Because we have no direct information of α, β, γ, ϵ, and ζ, our NMR model is only one of the many stereochemical solutions in the multi (α, β, γ, ϵ, ζ) space. One of the ways of narrowing down the possibilities is to energy minimize constrain to NOESY interproton distance criteria. This leads to Step 2.

Step 2. Choice of 60 Independent Constraints in the DNA Duplex. NOESY simulation provided a series of stereochemically allowed DNA models. These structures provided average values (±0.2 Å) for a set of interproton distances required for agreement with the NOESY data. Not all these distances estimated from the NOESY simulation are independent ones; e.g., when intranucleotide H8/H6(i)–H2′(i) and H8/H6(i)–H1′(i) are defined, other intranucleotide distances, i.e., H8/H6(i)–H2″(i), H8/H6(i)–H3′(i), etc., are automatically defined. Similarly, when internucleotide H8/H6-(i)–H1′(i − 1) and H8/H6(i)–H2″(i − 1) are defined, other internucleotide distances, i.e., H8/H6(i)–H2′(i − 1), H8/H6(i)–H3′(i − 1), are also defined. We, therefore, chose intranucleotide H8/H6(i)–H2′(i) and H8/H6(i)–H1′(i) and internucleotide H8/H6(i)–H2″(i − 1), H8/H6(i)–H1′(i − 1), H6(i)–CH_3(i + 1), and H8(A5)–CH_3(T6) as structural constraints for a given residue. This resulted in 60 interproton distances as structural constraints for the d(GA_4T_4C)$_2$. A complete list of constraints used and the deviations in each constraint in the final energy-minimized structure is given in the supplementary material. These 60 distances are used in the all-atom energy minimization as distance constraints [tied by a force constant K with a pseudopotential equal to $^1/_2K$-($d_{const} - d_{actual}$)^2]. Initially, K was set at 100 kcal mol^{-1} Å^{-2}, but when the system reached close to local minimum the value was reduced to 10 kcal mol^{-1} Å^{-2} (see the supplementary

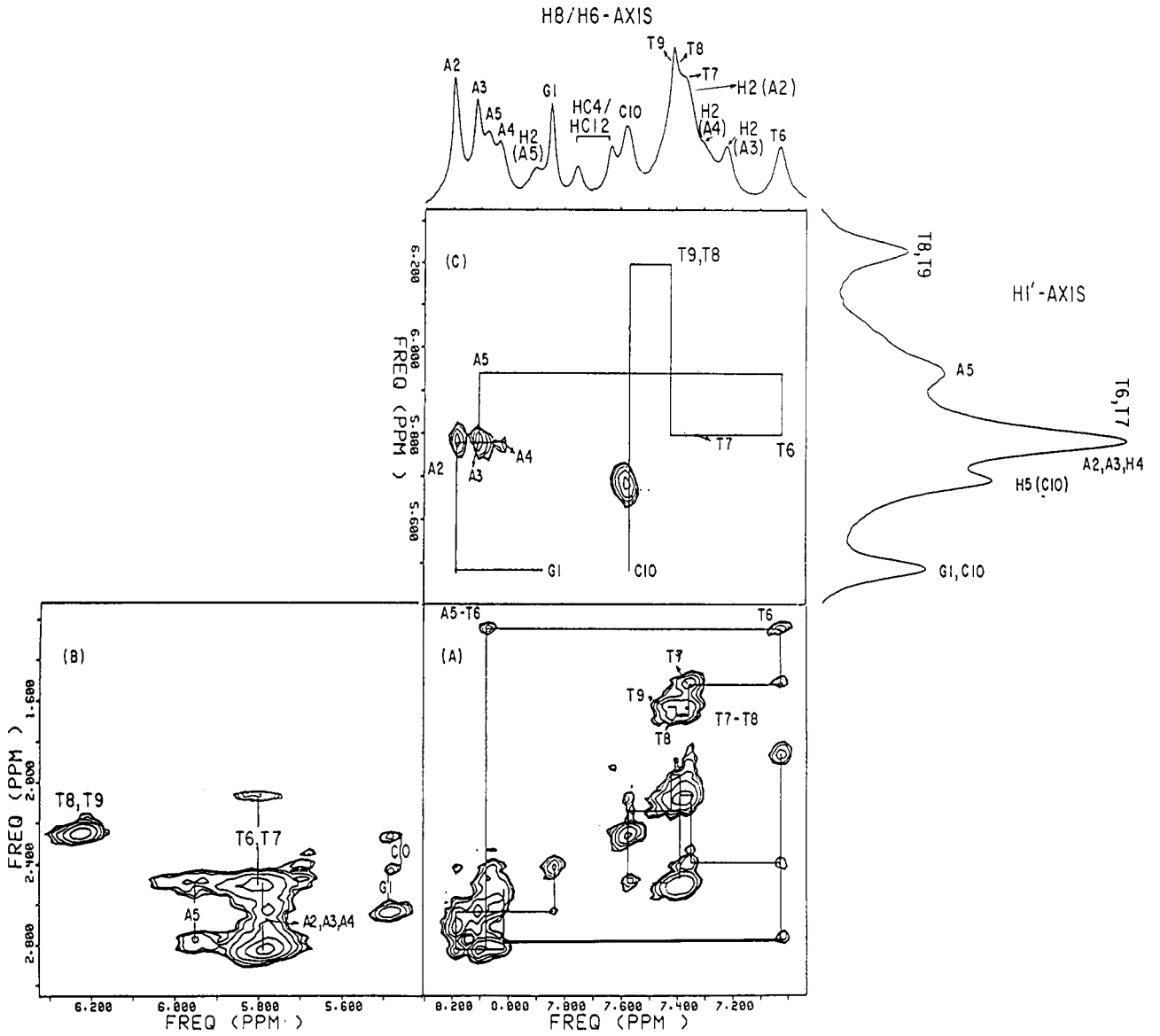

FIGURE 5: NOESY spectra for τ_m = 100 ms of the Dst2–d(GA_4T_4C) (1:1) complex in D_2O at 22 °C. (A) The H8/H6 vs H2′,H2″ cross section, (B) H1′ vs H2′,H2″ cross section, and (C) H1′,H5′ vs H8/H6 cross section.

material).

The energy minimization was performed in the Cartesian space by using the force field of Wiener et al. (1982). For energy minimization, Dst2 was docked in the minor groove spanning the 5 central A·T bps (Figures 6 and 7). It was our intention to examine the structural similarity of the NMR and NOESY constrained energy minimized model. Arnott and Hukin's (1972) B-DNA model was the starting structure of d(GA_4T_4C)$_2$ in the complex because in this model DNA interproton distances are far removed from those required by the NOESY criteria (i.e., in the NMR model). Minimization of this model is likely to enable somewhat unbiased search of the conformational space. Closeness (if observed) between the NMR and energy-minimized model should then be a real indication that in the neighborhood of the NMR model one can obtain an energetically stable structure that agrees with the NMR data. Indeed, we are able to obtain one energy-minimized model of Dst2–d(GA_4T_4C)$_2$ (1:1) complex that agrees with the NOESY data. In the energy-minimized model of the complex, we have the following drug–DNA distances: H2(A5/A15)---HC3/HC11 = 2.4 Å, H1′(T6/T16, T7/T17)---HC3/HC11 = 3.2–3.5 Å. This distance profile produces a NOESY pattern in agreement with the data in Figure 7.

Table II: Torsion Angles[a] (deg) of the NOESY Constrained Energy Minimized Structure of Dst2–d(GA_4T_4C)$_2$

	α	β	γ	δ	ϵ	ζ	χ
G1			58	142	175	261	250
			(36)	(144)	(176)	(245)	(254)
A2	292	182	57	135	173	261	245
	(322)	(180)	(36)	(144)	(176)	(245)	(259)
A3	294	180	59	133	174	258	248
A4	295	184	56	133	178	260	252
A5	291	177	58	119	176	260	252
	(322)	(180)	(36)	(144)	(177)	(248)	(259)
T6	295	175	61	130	177	262	240
	(317)	(181)	(45)	(132)	(177)	(254)	(251)
T8	294	179	58	128	176	261	244
T9	294	178	59	130	177	262	241
					(177)	(254)	
C10	291	180	58	126			235
	(315)	(181)	(45)	(132)			(246)

[a] Torsion angles of the NMR model are given the parentheses. In the NMR model two conformationally identical structural blocks are joined at the A5-T6 sequence constrained to the NOESY distance criteria.

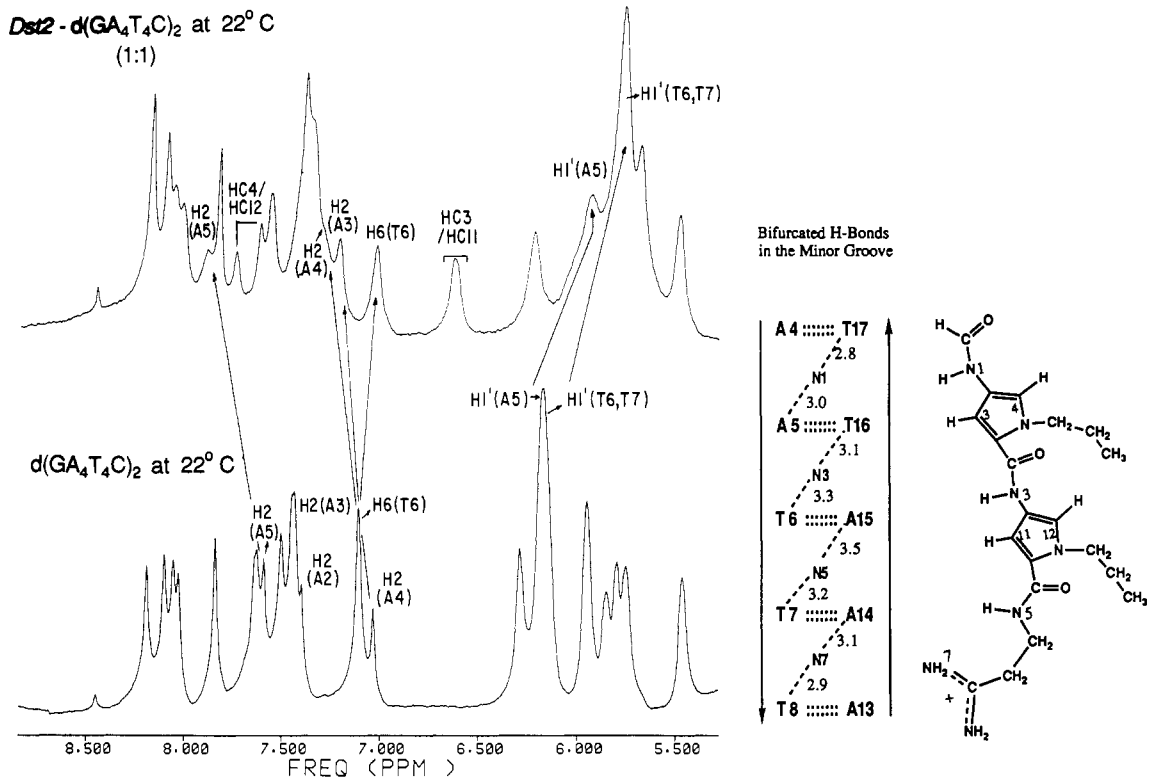

FIGURE 6: Sequence-specific changes in the chemical shifts of the H8/H6, H1′ proton of DNA upon Dst2 binding. Note that, upon drug binding, H2 of A4 and A5 move downfield while H2 of A2 and A3 remain essentially unchanged; H6 of T6 moves high-field. H1′ of A5, T6, and T7 move high-field. Other protons in the H8/H6, H2, H1′ region show very little change. Such a sequence-specific change in chemical shift is consistent with the hypothesis that Dst2 docks in the center of the minor groove of the $d(GA_4T_4C)_2$ duplex and forms bifurcated H bonds with 5 central A·T pairs, as shown in the diagram. Note that, Dst2 with two different groups at two ends of the molecule can also bind to the same 5 central bps in the reverse orientation. NMR data cannot distinguish between these two possible binding modes.

Table III: Comparison of Local Helical and Base Parameters for Free and Complexed $d(GA_4T_4C)_2$[a]

	tilt (τ) (deg)	roll (ρ) (deg)	twist (Ω) (deg)	slide (D_y) (Å)	rise (D_z) (Å)	Pr Tw[b] (ω) (deg)	buckle (bu) (deg)
G-C	0.6	3.4	37.3	−0.5	2.9	−15.2	−19.4
	(−0.6)	(−3.1)	(35.4)	(−0.4)	(3.3)	(−16.2)	(5.8)
A-T	−0.2	0.1	37.5	−0.3	2.8	−25.7	−6.7
	(−1.4)	(−2.8)	(35.0)	(−0.3)	(3.3)	(−20.8)	(−5.9)
A-T	−0.5	−2.3	39.3	−0.4	2.9	−23.8	3.2
	(−1.4)	(−2.8)	(35.0)	(−0.3)	(3.3)	(−20.8)	(−6.2)
A-T	−0.3	0.5	34.7	−0.4	3.1	−16.9	5.6
	(−1.4)	(−2.8)	(35.0)	(−0.3)	(3.3)	(−20.8)	(−6.6)
A-T	0.3	0.6	38.8	−0.5	3.1	−14.3	2.1
	(−0.1)	(−7.0)	(38.3)	(−0.3)	(3.4)	(−20.5)	(−6.9)
T-A	0.6	2.1	37.2	−0.5	3.0	−15.5	5.3
	(−1.4)	(−2.8)	(35.0)	(−0.3)	(3.3)	(−20.8)	(7.0)
T-A	0.8	2.9	32.8	−0.3	3.1	−17.9	4.0
	(1.4)	(−2.8)	(35.0)	(−0.3)	(3.3)	(−20.8)	(7.0)
T-A	1.8	3.2	36.4	−0.6	2.9	−17.7	3.0
	(1.4)	(−2.8)	(35)	(−0.3)	(3.3)	(−20.8)	(6.9)
T-A	0.7	2.7	35.7	−0.8	3.0	−19.4	7.6
	(1.4)	(−2.8)	(35)	(−0.3)	(3.3)	(−20.8)	(6.9)
						−12.7	13.9
C-G						(−16.1)	(5.9)

[a] Parameters are computed by the methodology of Bhattacharya and Bansal (1988). Complexed $d(GA_4T_4C)_2$ is the energy-minimized model of Figure 9. [b] Propeller twist.

Figure 8 displays the observed NOESY slices and theoretically constructed NOESY slices through H8/H6 protons for τ_m = 50 and 100 ms. Theoretical NOESY slices are computed with all nonexchangeable DNA and drug protons in the relaxation matrix (see Materials and Methods) for the NOESY-constrained energy-minimized model of the complex. Note that there is excellent agreement between experimental and theoretical data at 50- and 100-ms mixing times.

In the construction of the NMR model, the structure of the A/T block was first generated consistent with the NOESY data and then two rigid A/T blocks were joined at A5-T6. In the NOESY-constrained energy minimization, all Cartesian coordinates were allowed to change. As a result, in the energy-minimized model A(T) residues inside the A/T tract are conformationally different from each other while in the NMR model all A(T) in the A/T tracts are conformationally identical; see Table II for comparison of torsion angles in the NMR and energy-minimized model. However, there is a general similarity in conformations of the NMR and energy-minimized model, i.e., (i) all residues belong to the C2′-endo,anti domain

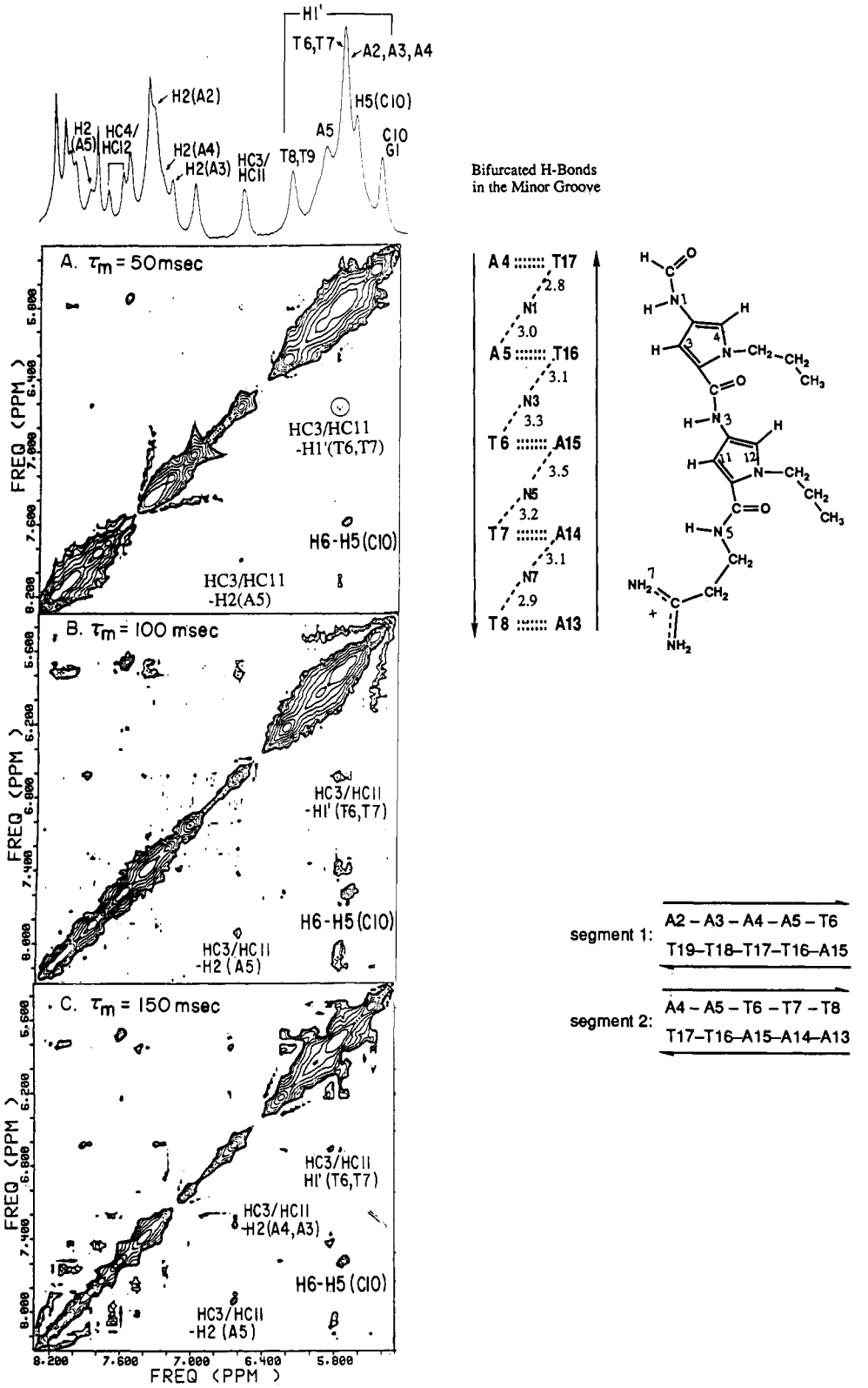

FIGURE 7: NOESY spectra showing HC3/HC11–H2(A) and HC3/HC11–H1′(A,T) as a function of τ_m. (A) For τ_m = 50 ms, HC3/HC11–H2(A5) appears as a prominent NOESY cross peak; compare with the H6–H5 (C10) cross peak. The HC3/HC11–H1′(T6,T7) cross peak is relatively weak. (B) For τ_m = 100 ms, HC3/HC11–H2(A5) and HC3/HC11–H1′(T6,T7) cross peaks become more intense. (C) For τ_m = 150 ms, an additional cross peak appears for HC3/HC11---H2(A4,A3) either due to spin-diffusion HC3/HC11 $\xrightarrow{2.5\text{ Å}}$ H2(A5) $\xrightarrow{3.5\text{ Å}}$ H2(A4) $\xrightarrow{3.5\text{ Å}}$ H2(A3) or due to a small population of the complex in which the drug spans segment 1 instead of segment 2 as shown in the diagram. In summary, sequence-specific drug–DNA NOESY data shown here clearly indicate that Dst2 is mainly located at the center of the minor groove of $d(GA_4T_4C)_2$.

(ii) ϵ and β are near-trans (180°) in both models, and (iii) P–O torsions (α, ζ) are $\bar{g}\bar{g}$ (245–262°, 290–320°). Note that, even though A's(T's) inside the A/T tract are conformationally different, they show only small variations.

In the NMR model, relation between two neighboring A/T blocks is described in terms of a reduced set of parameters, i.e., Δx, Δy, Δz, between two local frames defining two A/T blocks. For the energy-minimized model (all Cartesian coordinates being variables) the most appropriate description of the molecule is given in terms of local base and helical pa-

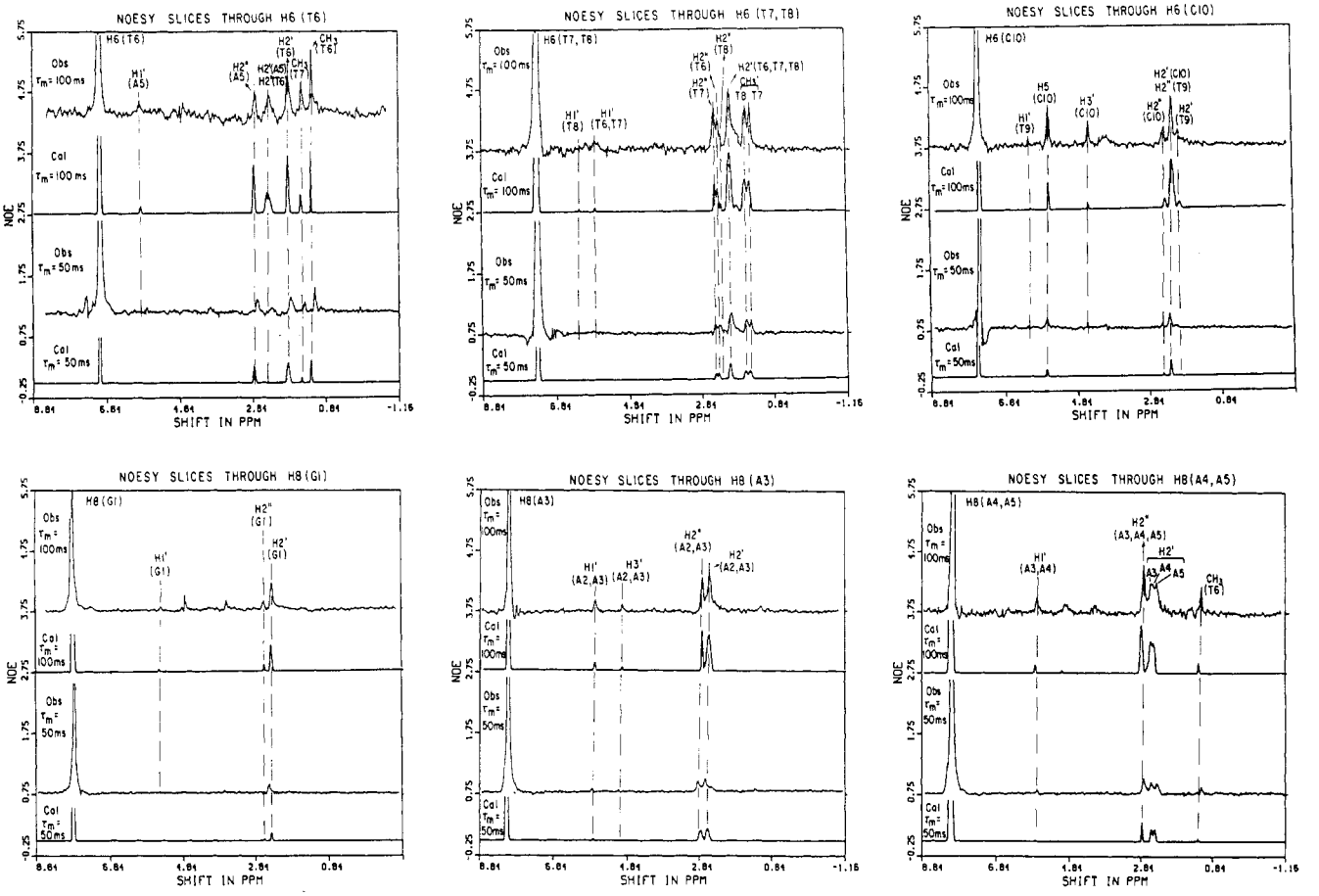

FIGURE 8: A set of observed and calculated 1D NOESY slices for the energy-minimized Dst2–d(GA_4T_4C)$_2$ (1:1) complex. In step 1, full-matrix NOESY simulation combined with molecular modeling (Gupta et al., 1988) resulted in a stereochemically allowed model for the Dst2–d(GA_4T_4C)$_2$ (1:1) complex that agreed with the NOESY data at τ_m = 150, 100, and 50 ms. This NMR model provided a set of average interproton distances as experimental structural constraints. In Step 2 these interproton distances were used as constraints to obtain an energy-minimized model for the Dst2–d(GA_4T_4C)$_2$ (1:1) complex. For the energy-minimized model NOESY intensities were computed by a full-matrix simulation method (Gupta et al., 1988). In order to account for the overlapping signal, we constructed an absorption spectrum with calculated NOESY intensities as peak heights and correspondingly assigning appropriate widths to match the observed spectrum. A correlation time of τ_c = 3 ns was used for the complex.

rameters (for a dimer sequence); these parameters were computed by the method of Bhattacharaya and Bansal (1988) and are listed in Table III for the NMR and energy-minimized model. Note the following similarities between the two models:

(i) A·T pairs are propeller twisted (Table III).

(ii) The A/T tract is straight (indicated by two tilt and role values); average local helical twist inside the A·T tract is 36° (Table III).

(iii) The presence of an array of interstrand bifurcated H bonds in the major groove (Figure 9A).

Analysis of the energy-minimized Dst2–d(GA_4T_4C)$_2$ (1:1) (the molecular model shown in Figure 9E) complex suggest that the main driving force of drug binding is sequence-specific (for A·T pairs) van der Waal interaction in the minor groove of B DNA. The array of bifurcated H bonds occurs as a consequence of favorable van der Waal interaction. The nature of H bonding between Dst2 and d(GA_4T_4C)$_2$ in this study and Dst3 and d($CGCA_3T_0CGC$)$_2$ in the single crystal (Coll et al., 1988) shows close similarity. It may be added that Kopka et al. (1985) also visualized a similar kind of H bonding between netropsin and d($CGCGA_2T_2CGCG$)$_2$ in the single crystal.

From our solution NMR study and the single-crystal studies of Coll et al. (1988) it may be concluded that Dst2 or Dst3 binding in the minor groove need not disrupt bifurcated H bonding of A·T pairs in the major groove. The most notable change in the structure of d(GA_4T_4C)$_2$ occurs in the P–P distances in the minor groove. Figure 9D compares the P–P distances (in the minor groove) for free d(GA_4T_4C)$_2$ and Dst2–d(GA_4T_4C)$_2$ (1:1) complex. Note that the P–P distance becomes smaller for the phosphate groups in two strands of the complex close to positively charged NH_2 groups due to favorable electrostatic interactions. Closing of the minor groove due to Dst2 binding is unidirectional because Dst2 has only a charged group at one end; for netropsin with charged groups at both ends, closing of the minor groove (if present) should be in both directions.

The results of our structural studies on the Ds2–d(GA_4T_4C)$_2$ (1:1) complex bears a close similarity with the conclusions derived by Pelton and Wemmer (1988). They determined the solution structure of the distamycin A–d($CGCGA_2T_2CGCG$)$_2$ complex using a combination of SKEWSY/NOESY and molecular mechanic methods. While we obtained the estimates of a set of interproton distances from the full-matrix NOESY simulation they obtained the same from the SKEWSY and NOESY data. Their structural analysis shows that the drug snugly fits into the central d(A_2T_2) and forms drug–DNA H bonds in the minor groove. The van der Waal contacts between the pyrrole ring protons and H2(A) are also implicated. They also conclude that drug binding does not cause any major alteration in the target DNA structure.

In our experiments, the Dst2 concentration is such that the drug can potentially span approximately half the possible A·T sites (5 out of 8 A·T pairs). EM studies on the bent 219-bp fragment of Kinetoplast DNA reveal an interesting role of drug

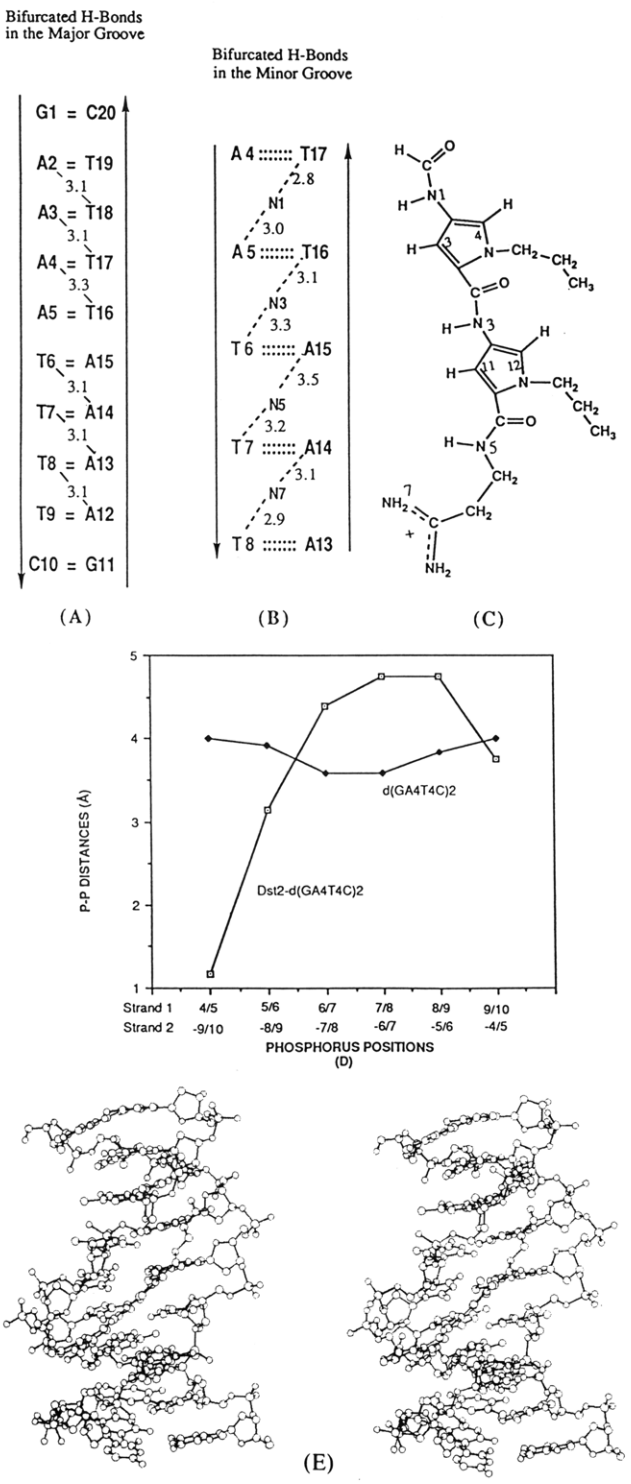

FIGURE 9: (A–C) Dst2 docked in the center of the minor groove of DNA. For the network of bifurcated H bonds in the major and minor groove. H bonding involves the N6(A) of one A·T pair and O4(T) of the next A·T pair across the strand in the 5′ → 3′ direction. In the minor groove, H bonding involves the N3(A) and O2(2) of DNA and the amide (N1, N3, N5) and amino N(7) of Dst2. Note that, drug binding does not break the bifurcated H bonds in the major groove of DNA (also present in free DNA). (D) A comparison of the P–P distances (in the minor groove) is graphically shown for free and complexed $d(GA_4T_4C)_2$. Note that the presence of a positively charged NH_2 group at one end of Dst2 tends to significantly narrow the minor group close to the site of interaction. (E) A stereopair of the NOESY constrained energy minimized structure of Dst2–$d(GA_4T_4C)_2$ (1:1).

concentration on DNA bending (Griffith et al., 1986). The 219-bp fragment of Kinetoplast DNA has 18 A/T tracts (each ~6 bp long—just enough for one distamycin), and therefore, this fragment offers 18 specific sites for drug binding. At a concentration of 1 drug/24 nucleotides distamycin can saturate all the specific binding sites. It appears from EM studies (Griffith et al., 1986) that at this range of drug concentration (reported for 1 drug/30–43 nucleotides) the 219-bp fragment is still bent. However, at concentrations of 1 drug/2.3–7 nucleotides, when the drug can potentially cover all the nucleotides, EM studies (Griffith et al., 1986) show that the drug removes the bending in the DNA molecule. In a personal telephone conversation, Dr. Griffith reaffirmed that diistamycin removes bending only at very high concentrations of the drug. It is apparent that only at low drug concentration (i.e., 1 drug/30–43 nucleotides) does EM monitor *A/T tract specific distamycin binding*, pertinent with the present study. And the fact that such sequence-specific binding does not alter the bent DNA conformation is in agreement with the results of the present study.

Conclusions. In summary, solution NMR [present work and Pelton and Wemmer (1988)] and single-crystal studies (Kopka et al., 1985; Coll et al., 1988) on DNA oligomers show that distamycin or its analogue does not cause a major alternation in the structure of the target DNA. The most prominent change common to drug binding is the opening of the minor groove of the A/T tract at the site of binding—mandatory for a stable drug–DNA complex. It turns out that the opening of the minor groove does not drastically release the propeller twist in the A·T pairs and hence it does not need to disrupt the bifurcated H bonds in the major groove (Coll et al., 1988).

Acknowledgments

We gratefully acknowledge Virginia Dollar for assistance in preparing the manuscript. We thank Dr. Manju Bansal for providing the base and helix parameters for Table III.

Supplementary Material Available

Lists of all-atom model calculations and of distance constraints for the $d(GA_4T_4C)_2$–Dst2 complex (13 pages). Ordering information is given on any current masthead page.

References

Arnott, S., & Hukins, D. W. L. (1972) *J. Mol. Biol. 81*, 93–101.

Bhattacharya, D., & Bansal, M. (1988) *J. Biomol. Struct. Dyn. 6*, 93–104.

Broido, M. S., James, T. L., & Keepers, J. W. (1985) *Eur. J. Biochem. 150*, 117–128.

Coll, M., Frederick, C. A., Wang, A., H., J., & Rich, A. (1987) *Proc. Natl. Acad. Sci. U.S.A. 84*, 8385–8389.

Griffith, J., Bleyman, M., Rauch, C. A., Kitchin, P. A., & Englund, P. T. (1986) *Cell 46*, 717–724.

Gupta, G., Sarma, M. H., & Sarma, R. H. (1984) *J. Biomol. Struct. Dyn.* 1457–1471.

Gupta, G., Sarma, M. H., & Sarma, R. H. (1985) *J. Biomol. Struct. Dyn. 2*, 1085–1098.

Gupta, G., Sarma, M. H., & Sarma, R. H. (1988) *Biochemistry 27*, 7909–7919.

Hagerman, P. J. (1985) *Biochemistry 24*, 7033–7041.

Hagerman, P. J. (1986) *Nature 321*, 1149–1150.

Keepers, S. W., & James, T. L. (1984) *J. Magn. Reson. 57*, 404–429.

Koo, H. S., Wu, A. M., & Crothers, D. M. *Nature 320*, 501–504.

Kopka, M. L., Yoon, C., Goosell, D., Pjura, P., & Dickerson, R. E. (1985) *Proc. Natl. Acad. Sci. U.S.A. 82*, 1376–1380.

Marini, J. C., Levene, S. D., Crothers, D. M., & Englund, P.

T. (1982) *Proc. Natl. Acad. Sci. U.S.A. 79*, 7664-7668.
Pelton, J. G., & Wemmer, D. E. (1988) *Biochemistry 27*, 8088-8096.
Saenger, W. (1984) in *Principles of Nucleic Acid Structures*, Springer-Verlag, New York.
Sarma, M. H., Gupta, G., & Sarma, R. H. (1988) *Biochemistry 27*, 3423-3432.
States, D. J., Haberkorn, R. H., Ruben, D. J. (1982) *J. Magn. Reson. 48*, 286-292.
Weiner, S. J., Kollman, P. J., Case, D. A., Singh, U. C., Ghio, C., Alagona, G., Proteta, S., & Weiner, P. (1984) *J. Am. Chem. Soc. 106*, 765-780.

Respiratory-Driven Na^+ Electrical Potential in the Bacterium *Vitreoscilla*†

Bassey J. S. Efiok and Dale A. Webster*
Department of Biology, Illinois Institute of Technology, Chicago, Illinois 60616
Received November 6, 1989; Revised Manuscript Received January 26, 1990

ABSTRACT: *Vitreoscilla* is a Gram-negative bacterium with unique respiratory physiology in which Na^+ was implicated as a coupling cation for the generation of a transmembrane electrical gradient ($\Delta\psi$). Thus, cells respiring in the presence of 110 mM Na^+ generated a $\Delta\psi$ of −142 mV compared to only −42 and −56 mV for Li^+ and choline, respectively, and even the −42 and −56 mV were insensitive to the protonophore 3,5-di-*tert*-butyl-4-hydroxybenzaldehyde (DTHB). The kinetics of $\Delta\psi$ formation and collapse correlated well with the kinetics of Na^+ fluxes but not with those of H^+ fluxes. Cyanide inhibited respiration, Na^+ extrusion, and $\Delta\psi$ formation 81% or more, indicating that $\Delta\psi$ formation and Na^+ extrusion were coupled to respiration. Experiments were performed to distinguish among three possible transport systems for this coupling: (1) a Na^+-transporting ATPase; (2) an electrogenic Na^+/H^+ antiport system; (3) a primary Na^+ pump directly driven by the free energy of electron transport. DCCD and arsenate decreased cellular ATP up to 86% but had no effect on $\Delta\psi$, evidence against a Na^+-transporting ATPase. Low concentrations of DTHB had no effect on $\Delta\psi$; high concentrations transiently collapsed $\Delta\psi$, but led to a stimulation of Na^+ extrusion, the opposite of that expected for a Na^+/H^+ antiport system. Potassium ion, which collapses $\Delta\psi$, also stimulated Na^+ extrusion. The experimental evidence is against Na^+ extrusion by mechanisms 1 and 2 and supports the existence of a respiratory-driven primary Na^+ pump for generating $\Delta\psi$ in *Vitreoscilla*.

The free energy change of respiration in aerobic prokaryotes is generally conserved by coupling it to the outward translocation of protons, thereby creating a H^+ electrochemical gradient ($\Delta\mu_{H^+}$)[1] across the cell membrane (Mitchell, 1976). The $\Delta\mu_{H^+}$ then mediates various endergonic transmembrane reactions such as ATP synthesis and substrate accumulation. Na^+ has been reported to play a similar role in several anaerobes which employ Na^+-transporting decarboxylases to transduce the free energy of decarboxylation to a Na^+ electrochemical gradient ($\Delta\mu_{Na^+}$) across the cell membrane during fermentative growth (Dimroth, 1980; Hilpert & Dimroth, 1982; Hilpert et al., 1984; Buckel et al., 1982). Recently, it has been reported that even in aerobic bacteria, Na^+ can replace H^+ as the primary coupling cation in energy transduction: the alkalotolerant marine bacterium *Vibrio alginolyticus* (Tokuda & Unemoto, 1982, 1984), a few other members of the *Vibrio* family (Udagawa et al., 1986; Tsuchiya & Shinoda, 1985), and the halotolerant bacterium BA1 (Ken-Dror et al., 1986) employ a respiratory-driven primary Na^+ pump to generate a $\Delta\mu_{Na^+}$. Except for BA1, Na^+ pumping generally predominates at alkaline pH conditions where the $\Delta\mu_{Na^+}$ is believed to help the cells overcome a deficit in $\Delta\mu_{H^+}$ caused by a reversed pH gradient.

Vitreoscilla, a Gram-negative filametous bacterium, is a strict aerobe found mostly in hypoxic habitats such as the benthic regions of fresh water sources (Nichols et al., 1986), and cow dung (Pringsheim, 1951). The respiratory chain is similar to that of the *Escherichia coli*; it has both cytochrome *o* and cytochrome *d* terminal oxidases, and quinol is the direct electron donor to the cytochrome *o* oxidase (Georgiou & Webster, 1987a,b). Other aspects of the bacterium's respiratory physiology are rather unique; for example, high levels of *Vitreoscilla* hemoglobin are found in its cytoplasm under hypoxic conditions. It has been suggested that this hemoglobin acts as an O_2 "storage trap" under these conditions (Wakabayashi et al., 1986). Second, *Vitreoscilla* cells are lethally sensitive to moderate concentrations of extracellular K^+, but they can be protected by Na^+ (Efiok and Webster, unpublished results). Finally, *Vitreoscilla* is a mild alkalophile which grows optimally at a pH of about 8.0–8.5 but can grow up to pH 9.5 (Lambda & Webster, 1980).

These observations prompted us to measure the key components of $\Delta\mu_{H^+}$ ($\Delta\psi_{H^+}$ and ΔpH) across the membrane of *Vitreoscilla*. Surprisingly, only a minimal $\Delta\psi$ was detected unless Na^+ was added to the assay medium, irrespective of

† This work was supported by National Institutes of Health Grant GM27085.

[1] Abbreviations: $\Delta\mu_{H^+}$, H^+ electrochemical potential gradient; $\Delta\mu_{Na^+}$, Na^+ electrochemical potential gradient; $\Delta\psi$, electrical potential gradient; TPP^+, tetraphenylphosphonium ion; $[Na^+]_o$, extracellular Na^+ concentration; $[Na^+]_i$, intracellular Na^+ concentration; pH_o, extracellular pH; pH_i, intracellular pH; CCCP, carbonyl cyanide *m*-chlorophenylhydrazone; DCCD, dicyclohexylcarbodiimide; DTHB, 3,5-di-*tert*-butyl-4-hydroxybenzaldehyde; BCECF, 2,7-bis(2-carboxyethyl)-5(6)-carboxyfluorescein.

0006-2960/90/0429-4734$02.50/0